Journal of Korean Powder Metallurgy Institute
Vol. 13, No. 5, 2006

Hydrogenation and Electrochemical Characteristics of Amorphous-nanostructured Mg-based Alloys

A. Gebert*, B. Khorkounov and L. Schultz
Leibniz-Institute for Solid State and Materials Research IFW Dresden, P.O. Box: 270016, 01171 Dresden, Germany
(Received September 1, 2006; Accepted October 2, 2006)

Abstract In the development of new hydrogen absorbing materials for a next generation of metal hydride electrodes for rechargeable batteries, metastable Mg-Ni-based compounds find currently special attention. Amorphous-nanocrystalline $Mg_{63}Ni_{30}Y_7$ and $Mg_{50}Ni_{30}Y_{20}$ alloys were produced by mechanical alloying and melt-spinning and characterized by means of XRD, TEM and DSC. On basis of mechanically alloyed Mg-Ni-Y powders, complex hydride electrodes were fabricated and their electrochemical behaviour in 6M KOH (pH = 14,8) was investigated. The electrodes made from $Mg_{63}Ni_{30}Y_7$ powders, which were prepared under use of a SPEX shaker mill, with a major fraction of nanocrystalline phase reveal a higher electrochemical activity for hydrogen reduction and a higher maximum discharge capacity (247 mAh/g) than the electrodes from alloy powder with predominantly amorphous microstructure (216 mAh/g) obtained when using a Retsch planetary ball mill at low temperatures. Those discharge capacities are higher that those for nanocrystalline Mg_2Ni electrodes. However, the cyclic stability of those alloy powder electrodes was low. Therefore, fundamental stability studies were performed on $Mg_{63}Ni_{30}Y_7$ and $Mg_{50}Ni_{30}Y_{20}$ ribbon samples in the as-quenched state and after cathodic hydrogen charging by means of anodic and cathodic polarisation measurements. Gradual oxidation and dissolution of nickel governs the anodic behaviour before a passive state is attained. A stabilizing effect of higher fractions of yttrium in the alloy on the passivation was detected. During the cathodic hydrogen charging process the alloys exhibit a change in the surface state chemistry, i.e. an enrichment of nickel- species, causing preferential oxidation and dissolution during subsequent anodization. The effect of chemical pre-treatments in 1% HF and in 10 mg/l YCl_3/1% H_2O_2 solution on the surface degradation processes was investigated. A HF treatment can improve their anodic passivation behavior by inhibiting a preferential nickel oxidation-dissolution at low polarisation, whereas a YCl_3/H_2O_2 treatment has the opposite effect. Both pre-treatment methods lead to an enhancement of cathodically induced surface degradation processes.

Keywords : Hydrogen absorbing materials, Mg-based alloys, Electrochemical characteristics

1. Introduction

In the development of new hydrogen absorbing materials for metal hydride electrodes of rechargeable Ni-MH batteries[1] Mg-Ni- based alloys find currently special attention. Those are closely related to the Mg_2Ni compound with a theoretical discharge capacity $C_{max} = 1000$ mAh/g corresponding to the formation of the complex hydride Mg_2NiH_4 with 3,6 wt.% hydrogen[2]. However, the measured discharge capacity of electrodes fabricated from microcrystalline Mg_2Ni is only 8 mAh/g[3]. This is the consequence of a slow hydriding kinetics mainly caused by the rapid formation of thin hydride layers on the large Mg_2Ni grain surfaces, which act as strong barriers for further hydrogen diffusion. Further microstructural refinement is necessary to improve the electrode performance. The C_{max} values

*Corresponding Author : [Tel : +49-351-4659-275/541; E-mail : gebert@ifw-dresden.de]

of electrodes made from mechanically alloyed nanocrystalline Mg_2Ni powders vary significantly ranging from about 100-150 mAh/g for the pure phase[4,5] to 636 mAh/g for Mg_2Ni intensively milled with Ni[6]. The measured values obviously depend not only on the alloy microstructure, but also on surface modifications and on the electrode preparation technique. Though these first studies on electrodes made from nanocrystalline or amorphous powders are promising with respect to the practically attained discharge capacities, one of the major problems is the low corrosion resistance at pH>14, which strongly limits the cycle life stability[7]. Various approaches have been followed for improving the cycle life of Mg-Ni- based electrodes[8]. Mainly compositional modifications with transition metals, Ti[9], Zr[10], Co[11], or Al[5] and rare earths[12] have been considered as useful ways, but also the preparation of composite materials, particle size control and chemical surface modifications[13,14].

In the present paper on fundamental studies on the alloys $Mg_{63}Ni_{30}Y_7$ and $Mg_{50}Ni_{30}Y_{20}$, which are known to exhibit a certain glass-forming ability[15], but mainly form an amorphous-nanocrystalline mixed structure by melt-spinning or mechanical alloying, regarding their suitability as new hydride electrode materials is reported.

2. Experimental

Elemental powders of Mg (99,8%, particle size 250 μm) and Ni (99,9%, particle size 300 mesh) and Y chips (99,9%, lumps size 20 mm) were used as starting materials for mechanical alloying of $Mg_{63}Ni_{30}Y_7$. Different milling conditions were employed:

a, using a Retsch planetary ball mill, model PM 4000, with a ball-to-powder ratio (BPR) of 13:1 and a rotation speed of 200 rpm; after each hour of milling the procedure was interrupted and the steel vials were cooled in a liquid nitrogen bath for 0,5 h.

b, using a SPEX shaker mill, model 8000, with a BPR of 10:1 at ambient temperature for 10-15 h in a continuous milling mode or up to 50 h in a discontinuous mode.

Ingots of the $Mg_{63}Ni_{30}Y_7$ and $Mg_{50}Ni_{30}Y_{20}$ alloys were prepared by induction melting in a purified argon atmosphere. From the master alloys, ribbons with a width of 5 mm and a thickness of about 30-40 μm were produced by single-roller melt spinning in a highly purified argon low-pressure atmosphere (Buehler melt spinner, 500 mbar Ar).

The mechanically alloyed powders and melt-spun ribbons were examined by means of X-ray diffraction (XRD) (Philips 1050, CoK_α radiation), transmission electron microscopy (TEM; Philips CM20FEG microscope), scanning electron microscopy (SEM) coupled with energy dispersive X-ray analysis (EDX) (Jeol JSM 6400 and Noran Instruments) and optical microscopy (Zeiss Axioskope 40). The thermal behaviour was examined by differential scanning calorimetry (DSC, Perkin Elmer DSC7) at a constant heating rate of 20 K/min.

Powder electrodes were fabricated by mixing the alloy powders with 50 wt.% of nickel powder and 10 wt.% polyvinyl alcohol solution (PVA) and pasting the mixture onto both sides of a nickel foam sheet. After drying, the coated foam sheet was cold pressed. Electrochemical tests regarding the hydride electrode performance were carried using a Potentiostat/Galvanostat EG&G Princeton Applied Research, model 273 A connected to a double compartment cell, in which the working electrode was separated from the counter electrode by a quartz porous frit. A Ni mesh was used as a counter electrode and a Hg/HgO, OH^- electrode (U(SHE) = + 0.0984 V) was the reference electrode (RE). The electrolyte used was nitrogen-purged 6 M KOH solution with pH = 14,8. For charge-discharge cycle tests, the electrodes were charged at $i_{charge} = -100$ mA/g for 10 h and then discharged at $i_{discharge} = 20$ mA/g up to a cut-off potential of -0,3 V within 10 cycles.

Fundamental electrochemical studies on ribbons

were performed in de-aerated 6 M KOH using a cell with platinum counter electrode and SCE reference electrode (U(SHE)=241 mV) connected to a Solartron SI 1287 Electrochemical Interface. Cyclic polarization tests at a scan-rate of 5 mV/s were performed starting from the OCP firstly towards anodic direction. For studying the effect of hydrogen pre-charging the ribbon samples were cathodically scanned (0.5 mV/s) from OCP to a potential corresponding to i= -25 mA/cm^2. This was followed by a galvanostatic step at i= -25 mA/cm^2 for 20 hours. After readjustment of the OCP for 30 minutes a fast cyclic polarization test was performed. Ribbons were chemically pre-treated either by short dipping in 1% HF solution or by repeated dipping and drying in 10 mg/l YCl_3/1% H_2O_2 solution. The hydrogen content [H] of all samples was determined using hot gas extraction (HORIBA-EMGA 621H hydrogen analyser).

3. Results and Discussion

3.1. Studies on mechanically alloyed powders

Fig. 1 shows the XRD patterns of $Mg_{63}Ni_{30}Y_7$ powders mechanically alloyed in a Retsch planetary ball mill up to 130 hours under cooling with liquid nitrogen and in a SPEX shaker mill up to 15 h at ambient temperature. The phase evolution during the mechanical alloying in a Retsch mill at very low temperatures requires long milling times due to a reduction of the alloying kinetics, but was found to be beneficial in comparison to milling at ambient temperatures with respect to the homogeneity of the final powders[16]. Continued milling at low temperatures leads to broadening of the starting elemental phase peaks and finally to the evolution of a broad diffuse halo revealing a progress in grain size refinement or amorphization. The refinement and alloying of Mg and Y proceeds considerably faster than that of Ni. Peaks corresponding to elemental Ni were detected within the entire alloying procedure, i.e. up to 130 h, while reflections of Y disappeared after 20 h and of Mg after 60 h of milling. After the final milling step besides the broad halo of an alloyed phase and the Ni reflections also peaks related with Y_2O_3 of a small intensity were identified in the XRD pattern. The oxygen content of the powder after 130

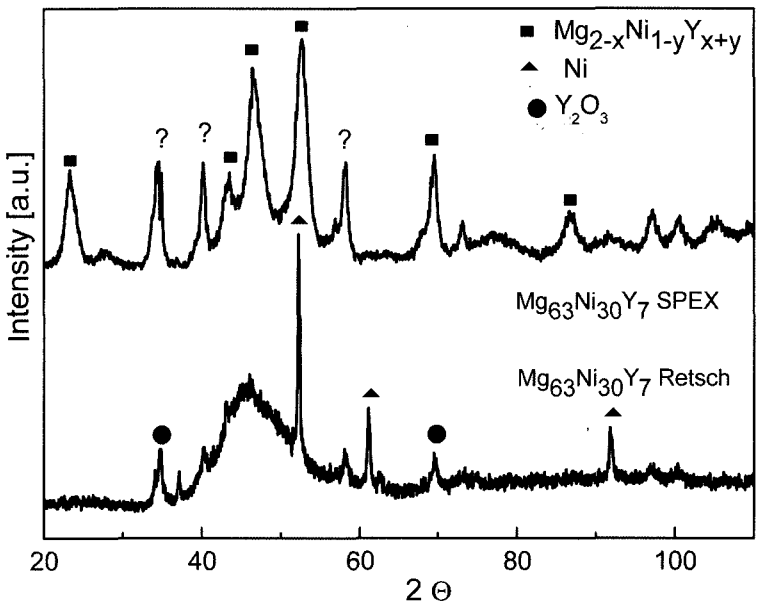

Fig. 1. XRD patterns of $Mg_{63}Ni_{30}Y_7$ powders mechanically alloyed in a Retsch planetary ball mill up to 130 hours under cooling with liquid nitrogen and in a SPEX shaker mill up to 15 h at ambient temperature.

h of milling was determined to be 1,02 wt.% (0,03 at.%), which is a typical contamination level. In contrast, the XRD pattern of $Mg_{63}Ni_{30}Y_7$ powder produced by continuous alloying in a SPEX mill exhibits diffraction peaks corresponding to the hexagonal Mg_2Ni main phase and further unknown phases. The broad peak shape indicates a small grain sizes (<100 nm) and large micro-strains in this phase. No reflections related to elemental Y or Y-containing intermetallic phases were detected in the XRD patterns. Thus, it is evident that Y was mainly alloyed into the Mg_2Ni-based phase. During discontinuous milling (1 h of milling followed by 1 h of rest) the first reflections of the Mg_2Ni-based phase were detected only after 50 h, while during the continuous milling the formation of this phase was already completed after 10 h. This suggests that the rise of the milling temperature during continuous alloying in a SPEX mill accelerates only the alloying kinetics, but does not change the phase formation mechanism. SEM observations of the powder milled continuously for 15 h revealed that the powder consists of a mixture of large particles with about 100 μm in diameter and of smaller particles with 5-40 μm, whereby the smaller grains are more homogeneous and have a smoother surface.

Additional TEM studies on the mechanically alloyed powders[16] revealed a mainly amorphous structure with few embedded nanocrystals (3-60 nm) for the Retsch-milled material, whereby a predominantly nanocrystalline structure and smaller fractions of amorphous phase were detected for the SPEX-milled material. Agglomerates formed by two types of nanocrystals were identified in the SPEX-milled powder: large fractions of smaller nanocrystals with an average size of 12-15 nm of a Mg-Ni-Y phase with lower Mg- and higher Y-content than the adjacent amorphous phase and small fractions of larger crystals (30-80 nm) of Y_2O_3 containing about 10 at. % Mg and 5 at. % Ni.

These microstructural differences are also indirectly evident from the thermal behaviour of

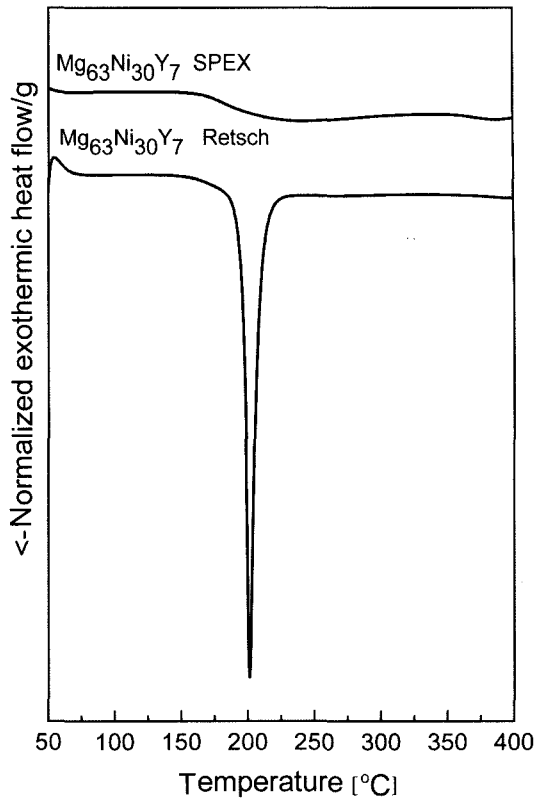

Fig. 2. DSC curves recorded at 20 K/min of $Mg_{63}Ni_{30}Y_7$ powders produced under different milling conditions: in a Retsch planetary ball mill up to 130 hours under cooling with liquid nitrogen and in a SPEX shaker mill up to 15 h at ambient temperature.

$Mg_{63}Ni_{30}Y_7$ powders prepared at different mechanical alloying conditions. Fig. 2 shows the DSC curves of the milling products. For both alloy powders, no endothermic event corresponding to a glass transition was observed. The SPEX- milled powder with major fraction of nanocrystalline phases exhibits only small exothermic signals within a wide temperature range. Those can be attributed to the crystallization of their small fraction of amorphous phase and also to nanocrystal growth. The Retsch-milled powder with predominantly amorphous fraction shows a single sharp exothermic peak at T_{max}= 200°C, which corresponds to the crystallization of the amorphous phase under formation of a hexagonal Y-containing Mg_2Ni-based nanocrystalline phase

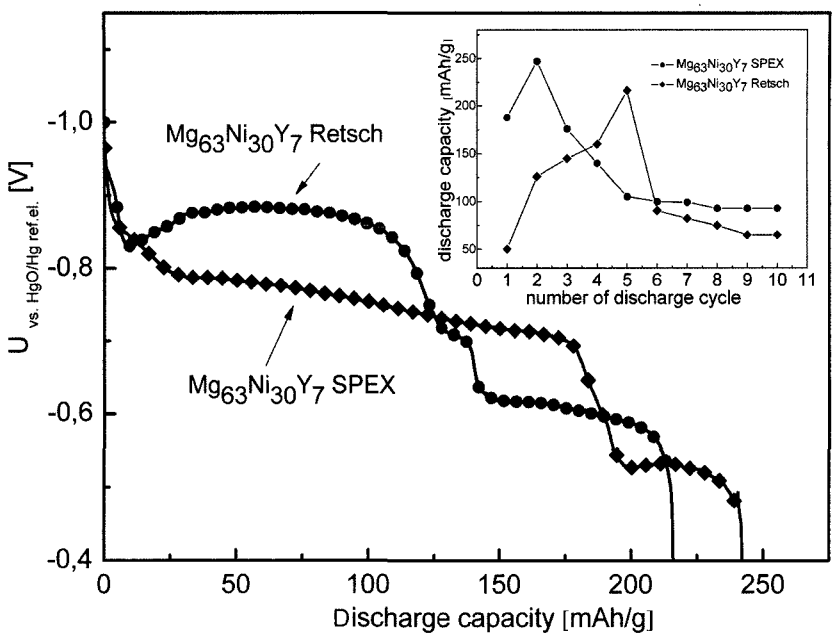

Fig. 3. Results of charge-discharge cycling tests on electrodes made from Retsch- and SPEX-milled $Mg_{63}Ni_{30}Y_7$ alloy powders in 6 M KOH: charge i_{charge} = -100 mA/g for 10 h; discharge $i_{discharge}$ = 20 mA/g. The discharge curves corresponding to the maximum discharge capacities are shown. *Inset*: dependence of the discharge capacity from the cycle number.

(grain size 8-12 nm)[16].

These mechanically alloyed $Mg_{63}Ni_{30}Y_7$ powders were subsequently used for the preparation of metal hydride electrodes and tested in a typical battery electrolyte, 6 M KOH. Fig. 3 summarizes results of galvanostatic cycling in terms of the discharge curves of the cycle where the maximum discharge capacity was attained and the discharge capacities plotted versus the cycle number (inset). For electrodes based on nanocrystalline SPEX-milled powder the maximum discharge capacity $C_{max.}$= 247 mAh/g is reached in the second cycle, and then the capacity decreased gradually in the following cycles. The electrodes made from mainly amorphous Retsch-milled powder require a longer activation procedure: a maximum discharge capacity $C_{max.}$= 216 mAh/g is obtained only in the fifth cycle. The longer activation period for electrodes made from amorphous powder corresponds to its stronger passivation ability as observed during anodic polarization[16]. The maximum discharge capacities obtained in the present study are higher than those for mechanically alloyed Mg_2Ni reported in the literature[4,5] and measured in the present work (140 mAh/g) and are also higher than those measured for nanocrystalline $Mg_{1.95}Me_{0.05}Ni$ (Me: Y, Ce, La, Nd; 180-200 mAh/g)[12] and $Mg_{2-x}Al_xNi$ (105-175 mAh/g)[5] and comparable with those for $Mg_{1.5}Mn_{0.5}Ni$ (241 mAh/g)[12]. However, longer cycling leads to electrode degradation, i.e. corrosion product formation, micro-cracking and particle pulverization. The electrodes studied here retain after 10 cycles about 30-35% of their maximum discharge capacity.

3.2. Studies on melt-spun ribbons

In order to analyze the origins of the low corrosion stability of the metastable Mg-Ni-Y alloys in the strongly alkaline battery electrolyte in more detail, investigations on melt-spun ribbons have been performed. Those exhibit - similar as the milled powders - a nanocrystalline-amorphous mixed structure[17], but also a clearly defined surface area to which

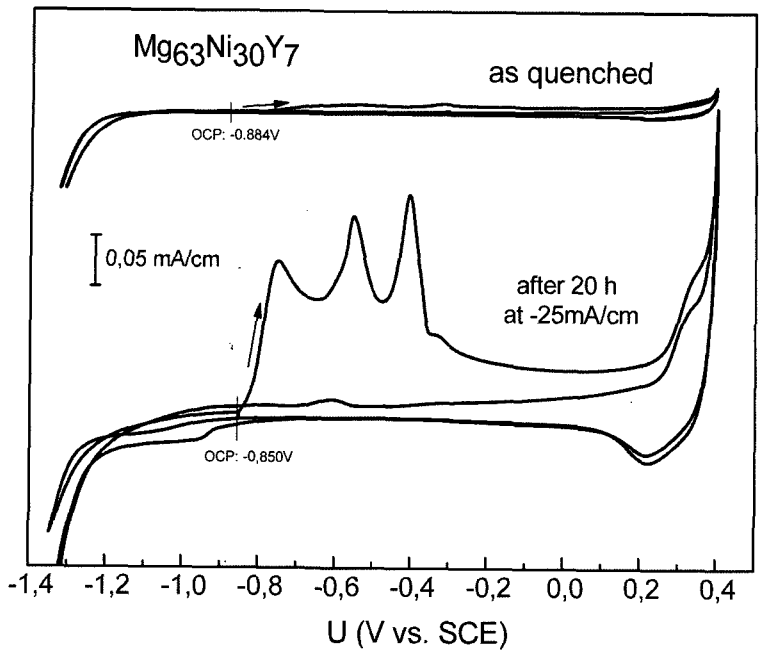

Fig. 4. Cyclic potentiodynamic polarization curves of $Mg_{63}Ni_{30}Y_7$ ribbon samples in 6 M KOH in the as-quenched state and after cathodic hydrogen pre-charging for 20 hours at i = -25 mA/cm².

measured currents can be directly related. Fig. 4 shows the cyclic potentiodynamic polarization curves of $Mg_{63}Ni_{30}Y_7$ ribbon samples in 6 M KOH in the as-quenched state and after cathodic hydrogen pre-charging for 20 hours at i = -25mA/cm². A very similar polarisation behaviour was observed for $Mg_{50}Ni_{30}Y_{20}$ ribbon samples (see in part in Fig. 6). The open circuit (OCP) or corrosion potentials of the untreated alloys establish at quite negative potentials owing to the main fraction of highly reactive components magnesium and yttrium. Upon beginning anodic polarisation two weakly pronounced oxidation peaks occur in the potential range up to -0,2 V mainly related to the nickel oxidation before a passive state is attained. Under free and low anodic polarisation conditions $Mg(OH)_2$ and $Y(OH)_3$ can spontaneously form as thin permeable films on the untreated alloy surface. Nickel anodically oxidizes initially under preferential formation soluble species, nickelite ions $HNiO_2^-$, thus being depleted from the alloy surface. Only upon further anodization solid nickel oxide species contributing to passivation can form by stepwise transformation to $Ni(OH)_2$ to Ni_3O_4 to Ni_2O_3 to NiO_2[18]. With progressing anodic polarisation the formation of $Mg(OH)_2$ and $Y(OH)_3$ is enhanced and governs the growth of a stable protective passive film at high potentials and in particular after the second cycle. During cathodic galvanostatic charging for 20 hours the ribbon samples absorb hydrogen, about 1.2 wt.%, for $Mg_{50}Ni_{30}Y_{20}$ and up to 1.1 wt.% for $Mg_{63}Ni_{30}Y_7$, under principal maintainance of their quenched-in structure. However, during charging their surface chemistry changes remarkably giving rise to strongly enhanced anodic current densities in the subsequent fast polarisation, in particular in clearly pronounced nickel oxidation peaks in the low polarisation regime. The cathodic loading further stabilizes $Mg(OH)_2$ and $Y(OH)_3$ at the ribbon surfaces, but also supports the gradual formation of "active nickel"[18] and metastable nickel hydrides, which are stepwise oxidized during the following anodic polarisation. The surface degradation during charging may in part explain the low amounts of absorbed hydrogen compared to the theoretically

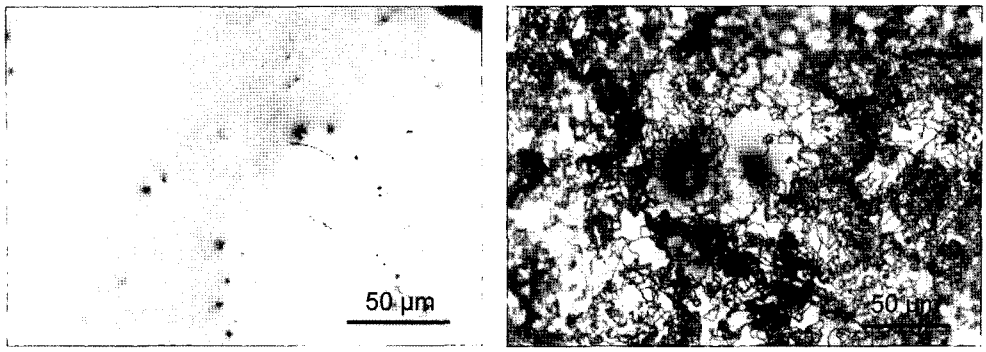

a, b,

Fig. 5. OM images of $Mg_{50}Ni_{30}Y_{20}$ ribbon surfaces (upper side) in the as-quenched state (a) and after treatment in 10 mg/l YCl_3/1% H_2O_2 solution (b).

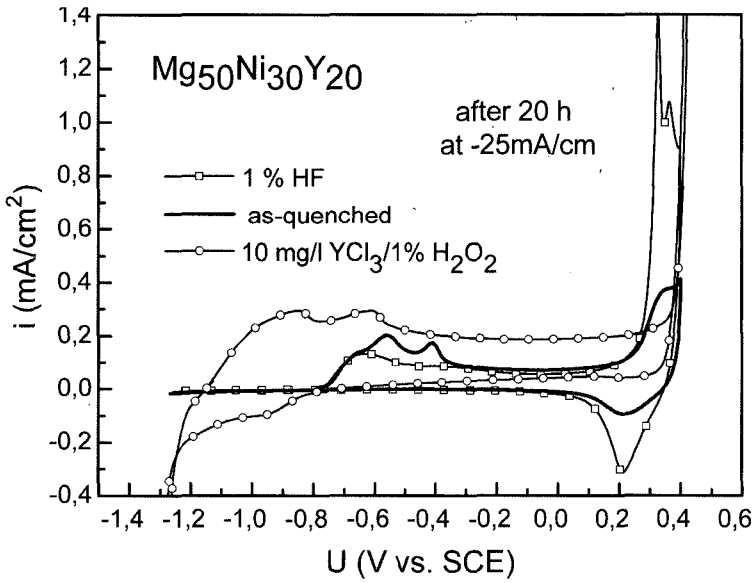

Fig. 6. Cyclic potentiodynamic polarization curves of $Mg_{50}Ni_{30}Y_{20}$ ribbon samples (in the as-quenched state and after chemical pre-treatments) in 6 M KOH after galvanostatic cathodic charging for 20 hours.

estimated values > 3 wt.%. Furthermore, a direct comparison of anodic polarisation curves of hydrogen-charged ribbon samples revealed for the $Mg_{50}Ni_{30}Y_{20}$ alloy reduced nickel oxidation currents and lower passive current densities compared to $Mg_{63}Ni_{30}Y_7$ indicating a positive effect of the alloy component yttrium in inhibiting the cathodic surface degradation process[17]. However, additional pre-modification of the alloy surface would be necessary to further reduce the surface corrosion during repeated cathodic and anodic polarisation in the battery electrolyte.

Therefore, in a first step selected chemical pre-treatments have been applied and their effect on the alloy stability was tested. Fig. 5 shows OM images of $Mg_{50}Ni_{30}Y_{20}$ ribbon surfaces (upper side) in the as-quenched state and after treatment in 10 mg/l YCl_3/1% H_2O_2 solution. The as-quenched ribbon surface appears rather smooth at this resolution, except a few single defects. No significant change was observed

after a short 1% HF solution exposure. On the sample surface treated in YCl_3/H_2O_2 solution a thick porous coarse-grained coating is formed. Further SEM-EDX analysis identified yttrium and oxygen species as main coating components. This layer was stable also after 24 hours exposure in 6 M KOH solution and during the polarisation experiments. However, a more detailed analysis of the ribbon surface topography in the sub-micron scale with atomic force microscopy (AFM) (not shown here) revealed a certain surface roughness of the as-quenched state corresponding to the nanocrystalline-amorphous structure. After both pre-treatments this surface topography was strongly modified, certainly a result of selective dissolution processes. Subsequent cyclic polarisation in strongly alkaline solution showed clearly that, a pre-treatment of melt spun amorphous-nanocrystalline $Mg_{50}Ni_{30}Y_{20}$ alloy samples with low concentrated HF solution can improve their anodic passivation ability by inhibiting a preferential nickel oxidation-dissolution at low polarisation. In contrast, a YCl_3/H_2O_2 solution treatment has the opposite effect. From Fig. 6 it is furthermore obvious that after both chemical pre-treatments and subsequent severe cathodic hydrogen charging of the ribbon samples the anodic peaks for the oxidation of nickel species are more pronounced and passive current densities at higher anodic potentials are partly increased. This suggests that those chemically generated surface modifications are not effective in inhibiting cathodic alloy degradation processes, but rather support them. Thus, these chemical pre-treatments are not suitable for increasing the corrosion resistance of Mg-Ni-Y alloys in a battery environment.

4. Summary and Conclusions

For hydride electrodes made from mechanically alloyed Mg-Ni-Y alloys with amorphous-nanocrystalline structure increased maximum discharge capacities were obtained compared to maximum values for other nanocrystalline Mg_2Ni-based alloys. A predominantly nanocrystalline structure yields higher values than a mainly amorphous structure. However, poor cyclic stability was observed due to severe electrode corrosion. Mg-Ni-Y alloys corrode in the strongly alkaline battery electrolyte under formation of $Mg(OH)_2$ and $Y(OH)_3$ passive layers. Increased yttrium content of the alloys is beneficial for inhibiting a preferential anodic nickel dissolution from the surface prior to and after cathodic hydrogenation. The applied chemical surface modification methods are not beneficial for remarkably improving the corrosion resistance. Other techniques, e.g. addition of further alloying additives or physically generated coatings may be more prospective.

Acknowledgements

The financial support of the German Research Foundation (DFG) under grant no. Ge 1106/3 is gratefully acknowledged. The authors are grateful to M. Johne, K. Hennig, M. Frey and S. Kuszinski for technical assistance, Ch. Mickel for TEM studies and M. Uhlemann and U. Wolff for fruitful discussions.

References

1. K. Hong: J. Alloys Comp., **321** (2001) 307.
2. J.J. Reilly: Z. Phys. Chemie NF, **117** (1979) 155.
3. N. Cui, B. Luan, H. K Lui, H. J. Zhao and S. X. Dou: J. Power Sources, **55** (1995) 263.
4. D. Mu, Y. Hatano and K. Watanabe: J. Alloys Comp., **334** (2002) 232.
5. A. Gasiorowski, W. Iwasieczko, D. Skoryna, H. Drulis and M. Jurczyk: J. Alloys Comp., **364** (2004) 283.
6. S. Nohara, N. Fujida, S. G. Zhang, H. Inoue and C. Iwakura: J. Alloys and Comp., **267** (1998) 76.
7. Y. Hatano, T. Tachikawa, D. Mu, T. Abe, K. Watanabe and S. Morozumi: J. Alloys Comp., **330-332** (2002) 816.
8. C. Rongeat, M.-H. Grosjean, S. Riggeri, M. Dehmas, S. Bourlot, S. Marchotte and L. Roue: J. Power Sources, **158** (2006) 747.
9. Y. Zhang, S.-K. Zhang, L.-X. Chen, Y.-Q. Lei and Q.-D. Wang: Int. J. Hydrogen Energy, **26** (2001) 801.
10. Y. Zhang, L.-X. Chen, Y.-Q. Lei and Q.-D. Wang: Elec-

trochim., Acta **47** (2002) 1739.
11. H. Yang, H. Yuan, Z. Zhou, G. Wang and Y. Zhang: J. Alloys Comp., **305** (2000) 282.
12. Z. M. Wang, H. Y. Zhou, Z. F. Gu, G. Cheng and A. B. Yu: J. Alloys Comp., **381** (2004) 234.
13. F.-J. Liu and S. Suda, J. Alloys Comp., **232** (1996) 212.
14. M. Dabala, K. Brunelli, E. Napoletani and M. Magrini: Surface and Coating Technology, **172** (2003) 227.
15. S. G. Kim, A. Inoue and T. Masumoto: Mater. Transactions JIM, **32** (1991) 609.
16. B. Khorkounov, A. Gebert, Ch. Mickel and L. Schultz: J. Alloys Comp., **416** (2006) 110.
17. A. Gebert, B. Khorkounov, U. Wolff, Ch. Mickel, M. Uhlemann and L. Schultz: J. Alloys Comp., **419** (2006) 319.
18. M. Pourbaix, Atlas of Electrochemical Equilibria in Aqueous Solutions, Pergamon Press Oxford, 1966.